https://doi.org/10.5194/nhess-2022-184
Preprint. Discussion started: 20 July 2022

Natural Hazards and Earth System Sciences
Discussions

Antecedent rainfall as a critical factor for the triggering of short-lived debris flows in arid regions

Shalev Siman-Tov[1], Francesco Marra[2]

[1]Geological Hazards Division, Geological Survey of Israel, Jerusalem, 9692100, Israel
[2]Institute of Atmospheric Sciences and Climate, National Research Council, Bologna, Italy

Correspondence to: Shalev Siman-Tov (shalevst@gsi.gov.il)

Abstract. In arid regions, debris flows are occasionally observed when torrential rainfall hits steep slopes with unconsolidated materials. Despite the important related hazards, not much is yet known about the critical rainfall conditions for debris flow initiation in dryland areas. In this study, we use high-resolution digital surface models and weather radar rainfall estimates for the detection and characterization of triggering and non-triggering storms. We focus on the arid slopes of the Dead Sea north-western margins and use the differences of digital surface models to identify deposits from over 40, relatively small, short-lived debris flows (SLDFs) occurred between 2013 and 2019. We divide them into four groups based on their spatial distribution and triggering period, and identify the most likely triggering storm for each group. Using high-resolution weather radar data we show that the SLDFs were likely initiated by an intense convective cell (lasting 20 to 45 min) which was preceded by significant rainfall amounts (8-12 mm) delivered during the storm. Comparing triggering and non-triggering storms, we observed that rain intensity alone is insufficient to explain the phenomena, and discuss the possibility that antecedent rainfall could represent a critical factor for the triggering of SLDFs in steep slopes of arid environments.

1 Introduction

Debris flows (DF) are gravity driven, downslope flows of water and sediment mixtures (Takahashi, 2014; Iverson, 1997). They constitute one of the most impactful natural hazards in mountainous regions, with casualties and damage to infrastructures. Debris flows commonly follow pre-existing channels and often end at lower gradients, where lobes of sediments are deposited at the mountain front. Cohesionless sediments that cover steep mountain slopes (e.g., colluvium or pyroclastic deposits) usually provide the debris material. The typical morphological characteristics of DF include levees along the channel sides, terminal lobes, coarse and poorly sorted grains, and U-shape flow channel with a low depth/width ratio (Costa, 1988; Pierson, 2005; Wells and Harvey, 1987). Debris flows are typically triggered by heavy precipitation or, more rarely, by sudden snow or ice melt in mountainous and volcanic areas. Short-duration convective storms constitute a key factor because high rain intensities may easily exceed the soil infiltration capacity causing surface runoff, leading to the triggering (Church and Miles, 1987; Iverson, 2000; Mostbauer et al., 2018; Dunkerley, 2021).

https://doi.org/10.5194/nhess-2022-184
Preprint. Discussion started: 20 July 2022


Natural Hazards and Earth System Sciences Discussions

Debris flows are common in temperate regions, probably because rainfall is the most common triggering factor (Caine, 1980). Nonetheless, DFs can also occur in arid and semiarid regions (Webb et al., 1989; Blackwelder, 1928; Stolle et al., 2015; Coe et al., 1997), as a result of the heavy rainfall extremes characterizing these areas (Marra and Morin, 2015) and of the quick runoff response typical of arid and unvegetated soils (Zoccatelli et al., 2019). For example, DFs were extensively studied in the semiarid to arid regions of the Grand Canyon slopes in northern Arizona, where they mostly occur when runoff triggers failures in colluvium during intense rainfall (Griffiths, 2004; Melis et al., 1994; Webb et al., 1989). Based on the available data, sustained intensity exceeding 20 mm h^{-1} and a total rainfall of 25 to 50 mm can be considered as the minimal threshold for DF triggering in this area (Melis et al., 1994; Webb et al., 1989; Melis and Webb, 1993).

The steep arid slopes of the Eastern Judean desert, on the western margins of the Dead Sea, are populated by a few human settlements, main roads and nature reserve infrastructures, so that DF activity can be particularly dangerous. In addition to their destructive potential, DFs have here a major influence on slope morphology and alluvial fan build up (Ben David-Novak et al., 2004; Ben David-Novak, 1998; Ahlborn et al., 2018; Enzel, 2001). Ahlborn et al. (2018), in particular, examined graded layer deposited during the Holocene associated to DFs, and observed periods with drier conditions and increased DF activity and periods with wetter conditions and lower DF activity. They associated this counter intuitive observation to changes in the synoptic conditions of the Eastern Mediterranean, raising the question whether the future occurrence frequency of DF, and therefore of the related hazards, could be affected by the ongoing climate change. While most of the critical environmental conditions for DF triggering are met, e.g., unconsolidated sediments on steep slopes, it seems that the most limiting factor in this area is precipitation (Ben David-Novak et al. 2004). The only studies about modern DFs in the area focused on a few rainstorms occurred between the years 1987-1997 (Ben David-Novak, 1998; Ben David-Novak et al., 2004). Using field surveys, aerial photos and rainfall estimates from rain gauges and weather radar, they suggest that minimum conditions for DF triggering consist of rainfall intensity exceeding 30 mm h^{-1} for duration of at least one hour. Nevertheless, the typical lifetime of convective cells in the area is shorter (around 20-40 min according to Belachsen et al. (2017)) and the effect of antecedent rainfall was not directly considered (Ben David-Novak et al., 2004).

An improved knowledge of the rainfall characteristics leading to DFs in arid regions is critical for the understanding of the triggering mechanisms and for improving our ability to provide effective early warnings. In this paper we aim at improving our understanding of the critical conditions for DF triggering in arid areas by combining high-resolution topography models, field surveys, and an advanced archive of high-resolution radar rainfall estimates which comprises both triggering and non-triggering events.

The paper is organized as follows. After introducing the reader to the study area (Section 2), we present our mapping of DFs in the study area (Section 3) and the identification of the most likely triggering rainfall (Section 4). We close by discussing the role of antecedent rainfall for DF triggering and the potential implications for DF frequency in the region (Section 5). We close with a collection of the main conclusions (Section 6).

https://doi.org/10.5194/nhess-2022-184
Preprint. Discussion started: 20 July 2022


Natural Hazards and Earth System Sciences Discussions

2 Study Area

2.1 Geography and geological settings

The study area is located on the east side of the northern Judean desert, on the northwestern escarpment of the Dead Sea basin (Fig. 1). We focus on the portion of the escarpment limited to the north by the Og Wadi and to the south by the Hever Wadi (Fig. 1). The slopes are mostly composed of carbonate rock layers including hard limestone and dolomites, interbedded with weak marl layers. These exposed carbonate rocks of the Judean Group units deposited on the regional carbonate platform during the Cretaceous (Sneh et al., 2000; Raz, 1983; Mor, 1987; Roth, 1969).

The slope angle is usually gentle (5°-30°) at the bottom and becoming steep (>30°) or vertical at its upper parts. This is a result of normal faulting followed by ongoing erosional processes along the margins of the Dead Sea basin since the late Miocene to early Pliocene (Garfunkel and Ben-Avraham, 1996; Garfunkel et al., 1981; Haviv et al., 2006). In many places along the lower parts of the escarpment, the carbonate rock slopes are covered by lacustrine and fluvial sediments, deposited during high lake stands in the Pliocene-Pleistocene periods (Bartov et al., 2002, 2007; Sneh, 1979; Begin et al., 1980). Many of these sediments are soft and/or cohesionless, and together with other colluvial deposits constitute the typical source material of DFs (Ben David-Novak et al., 2004).

2.2 Rainfall and weather systems

In the study area, the average annual precipitation ranges between 50 to 100 mm, based on constantly recording rain gauges for the years 1991-2020 (https://ims.gov.il/en/ClimateAtlas; see Fig. 1 for station locations). This variation in precipitation has a clear geographic gradient, with lower amounts observed in the southern part, caused by the decreasing frequency of precipitation, and in the eastern part, caused by the orographic shading of the Judean mountains. The rainy season is between October to May, with more frequent rainstorms during the winter (December to February), generally related to Mediterranean cyclones, and some less frequent, but more intense rainstorms during the autumn and spring months, generally related to Active Red Sea Troughs (ARST). While Mediterranean cyclones are characterized by regional scale rainfall that decreases southward and eastward in the study area, ARSTs produce heavy and localized convective rain cells which tend to occur more uniformly across our domain (Armon et al., 2019; Hochman et al., 2022). On rare occasions, Tropical Plumes may hit the region with large amounts of precipitation at the regional scale (Tubi and Dayan, 2014).

https://doi.org/10.5194/nhess-2022-184
Preprint. Discussion started: 20 July 2022

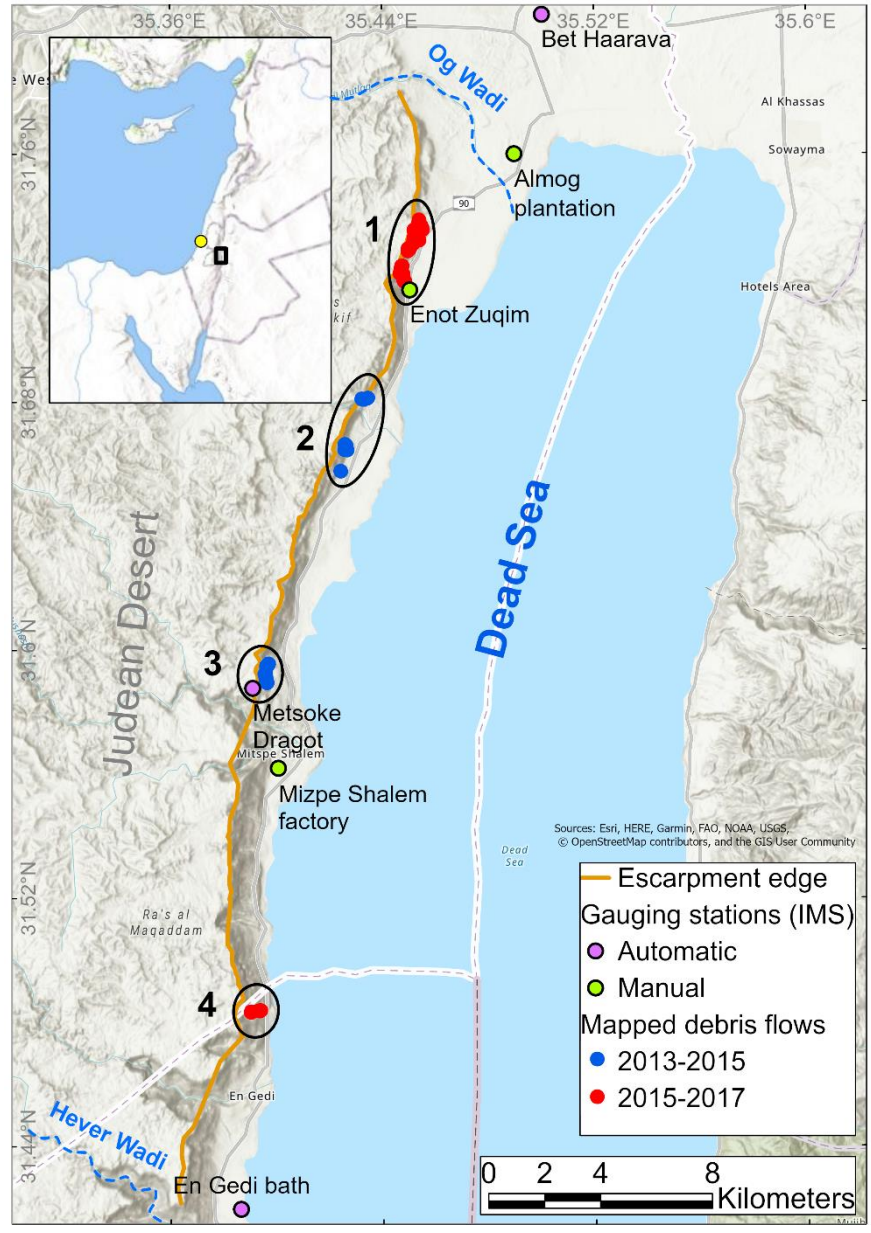

Figure 1: Map of the study area. An inset shows the location of the study area (black rectangle) and of the weather radar (yellow point) on the eastern Mediterranean map. The 43 short-lived debris flow deposits were mapped using elevation-difference maps from the years 2013-2015 (in blue) and 2015-2017 (in red). The deposits were classified into four groups (black ellipse). Rain gauge stations of the Israel meteorological service are marked in purple and green points for automatic (10-min) and manual (daily) stations, respectively.

https://doi.org/10.5194/nhess-2022-184
Preprint. Discussion started: 20 July 2022


Natural Hazards and Earth System Sciences Discussions

3 Debris flows detection and characterization

3.1 Mapping methods

Aiming to detect modern, natural changes resulting from mass-wasting processes along the studied escarpment, we compared aerial photos and high-resolution digital surface models (DSM) available for the years 2013-2019. The DSMs are the product of airborne light detection and ranging (LiDAR) scans, having spatial resolution of 0.5 m pixel^{-1} with spatial uncertainty <1 m. In the vertical dimension, the DSMs absolute elevation error is <0.35 m. We obtained DSMs of every second year: 2013 (scan date May 29-31, 2013), 2015 (Apr-May 2015), 2017 (May 12, 2017), 2019 (Sep 29-30, 2019). In order to identify topography changes, we subtract the earlier DSM from the more recent one. The new raster of elevation-differences should have positive values if material added, negative for deficiency, and around zero for no change. In general, this is the case apart from two exceptions: 1) the average difference value for stationary areas is non-zero, suggesting a vertical offset of a few tens of centimeters; 2) noisy results around high relief lines (cliffs). The first issue, probably caused by a systematic error of the DSM elevation, is expected to have a minor influence on our results: to ensure a better detection we computed the mean offset by averaging several stationary areas and subtract it from the elevation-difference map. The second issue mostly affects the cliff area, and the cliff lineaments in particular, and consists of noisy raster values (neighboring cells with values above and below zero). This artifact is not expected to affect our detection, because DFs are recognized by nearby regions with similar values, so that noisy areas can be easily excluded. However, some tiny SLDF deposits are possibly missed by this procedure, especially those with area smaller then ~25 m^2 and average thickness smaller than ~0.6 m.

In order to narrow our uncertainty in the estimated time of triggering (otherwise only limited by the time interval between airborne LiDAR scans), we used orthophotos, media and social network documentation. In terms of aerial photos, we mostly use geometrically corrected (orthophotos) with resolution of 0.25 m pixel^{-1}, from the years 2015 (photos taken in Jun-Jul 2015) and 2016 (photos taken Apr 15-30, 2016). Nevertheless, for most cases, the exact timing of the DF triggering was unknown and we had to identify the most probable triggering date as described below.

3.2 Identified debris flows and field observations

We identified 45 slope deposits along the steep escarpment of the study area that were resulted from landslides occurred between the years 2013-2019. Two of these deposits were classified as rockfalls related to the escarpment cliffs. The other 43 deposits are located along small ephemeral streams that drain the cliff area above them. This suggests that they were mobilized by flow events and therefore considered as short-lived debris flows (SLDFs). We define SLDFs as small-size DFs, having a runout distance between the source location and deposit of a few tens of meters. Although during the studied period (2013-2019), only SLDFs could be clearly mapped, longer runout distance DFs from past events are observed in the study area. In principle, it is possible that larger DFs did occur during the studied period (2013-2019), but subsequent road construction and floods blurred the DF tracks. This made it impossible for us to detect them by means of elevation-difference maps and to verify

https://doi.org/10.5194/nhess-2022-184
Preprint. Discussion started: 20 July 2022


Natural Hazards and Earth System Sciences Discussions

the nature of the phenomena (e.g., distinguishing between DF and flash floods) based on field surveys. This is to emphasize, that although the studied DFs are relatively small, their triggering mechanism is similar to potentially more hazardous DFs. All the mapped SLDFs in this study are of the first to second stream order, following the "top down" system division. Their drainage basins are extremely small, usually limited to the cliff itself or to a kilometer west of the clifftop at most. The spatial extent of each SLDF deposit was mapped into a polygon based on the elevation-difference maps (positive values for added material). These polygons were primarily grouped according to the time interval they were triggered (two years intervals based on the LiDAR scans): 17 SLDFs between 2013 and 2015, 26 SLDFs between 2015 and 2017, while no deposits were identified for the period 2017-2019 (Fig. 1). The areal extent of each SLDF deposit ranges between 10 and 1000 m^2 with an average value of 150 m^2 and elongated shapes of ~30 m in length and ~5 m in width.

Aiming to verify that the mapped deposits are indeed the result of SLDFs, we explored their structure and morphology in the field (Fig. 2). In many cases, the SLDFs are located on very steep slopes (20°-40°) with limited access. All mapped deposits and their related upstream erosional scours (i.e., depressions along the streams where the missing material is the source for the debris material) are located along or at the edge of short ephemeral streams that drain the cliff. The deposited sediments are poorly sorted, a principal characteristic that distinguished DFs from water-laid sediments. Distal lobes, also known as depositional lobes, are observed for all the mapped deposits at the toe of the flow. For some cases, also side lobes are observed upstream, along the flow path (Figs. 2e-2f). Levees, usually a few tens of centimeters high, are occasionally observed on both sides of the channel; although they are barely seen in the elevation-difference maps, in the field the greyish levees are clearly distinguished from the surrounding brownish colluvium (Fig. 2d). These levees consist of relatively large fragments, similar to those found in the lobes. All these elements suggest these deposits were caused by SLDFs.

For most of the mapped SLDFs, the deposits consist of angular dolomite and limestone fragments that reflect the upper cliff composition. In fact, it seems that the source for the debris material is the talus at the base of theses cliffs. Differently, in fewer cases (N=6) located at the bottom of a lower step on the escarpment, the deposits consisted of rounded fragments, apparently derived from the nearby cliff of lacustrine and conglomerate sediments. These same two sources of debris materials were also reported by previous studies in the region (Ben David-Novak et al., 2004).

We divided the mapped SLDFs into four groups based on the triggering time interval and on their spatial distribution across the study area, with the reasonable assumption that each group has been triggered by an individual convective cell (Fig. 1). While it is in theory possible that nearby SLDFs were triggered by different storms over a short period of time, we deem this possibility highly unlikely due to the rare occurrence of DFs in the region. Conversely, a specific storm, that may last for a few days, could represent the trigger of several groups. However, since the distances between groups observed in the same 2-year time intervals is always greater than 8 km, and the typical scale of convective cells in the region is smaller (Belachsen et al., 2017; Marra and Morin, 2018), these groups were likely triggered by different convective cells. As we will see, this is

https://doi.org/10.5194/nhess-2022-184
Preprint. Discussion started: 20 July 2022

Natural Hazards and Earth System Sciences
Discussions

155 possibly the case of our groups one and four, which occurred in the northern and southern parts of the study area, respectively (Fig. 1).

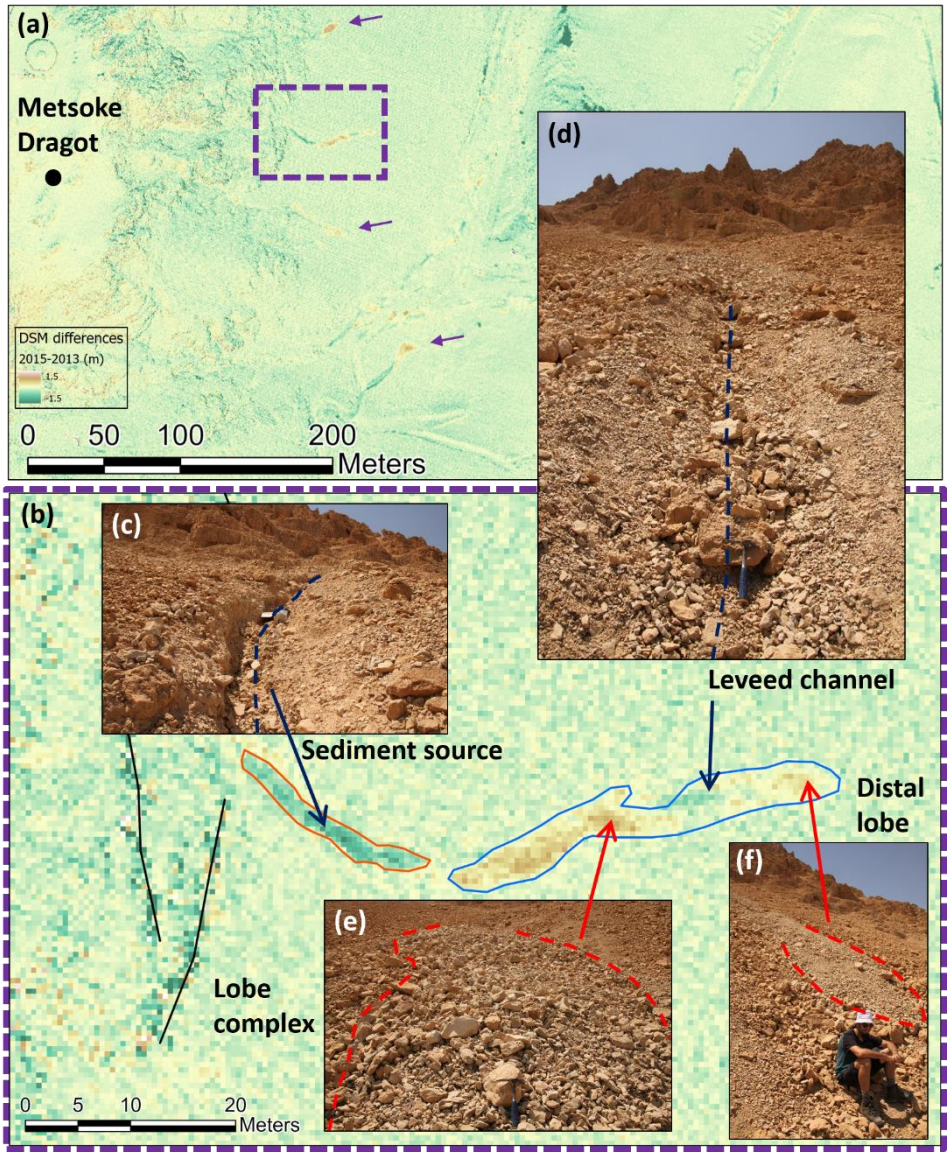

Figure 2: Mapping and characterization of short-lived debris flows (SLDFs) in the field and the topographic models. (a) Natural changes in the steep slope east to Metsoke Dragot village as reflected from the elevation-difference map of the years 2013-2015. Brown
160 shades suggest newly deposited materials while dark green shades represent new depressions. More details on the SLDF in the purple rectangle are shown in panels b to f. Arrows mark three additional SLDF deposits. (b) Zoom in to the SLDF area, where the source of the debris material and the elongated deposits are well seen in the map. Upper slope Cliffs (black lines) are noisier in the difference maps. (c) A channel (dashed line shows its path) incised in the unconsolidated colluvium. (d) The SLDF channel with parallel levees on its margins. (e) Deposits of the lobe complex. (f) The distal lobe.

https://doi.org/10.5194/nhess-2022-184
Preprint. Discussion started: 20 July 2022


Natural Hazards and Earth System Sciences Discussions

4 The triggering rainstorms

4.1 Rainfall data

Our mapping of natural changes along the steep escarpment between the years 2013-2019 suggests that the majority of mass wasting events were caused by SLDFs. We used both rainfall stations located within or in close proximity to the study area and the weather radar of the Israeli meteorological service (Fig. 1) to identify and characterize the triggering storms. We used the rainfall data from two types of stations (https://ims.gov.il/en/stations) as shown in Fig. 1: 1) Automatic rain gauges with a time resolution of ten minutes (from north to south: Bet Haarava, Metsoke Dragot, En Gedi bath); 2) daily rain gauges (from north to south: Almog plantation, Enot Zuqim, Mizpe Shalem factory).

The weather radar (https://ims.gov.il/en/node/193) gives rainfall intensity maps every five minutes at 500 m resolution, and allows spatial analysis of the event. In particular, weather radar data is essential to capture the DF triggering rainfall conditions especially in convective environments (Marra et al., 2016; Destro et al., 2017). Weather radar data was provided by the Israel Meteorological Service and elaborated following the procedures described in Marra et al. (2022), which include physically-based corrections and empirical adjustments based on rain gauge climatology. In addition, in order to reduce the bias typically observed in our study area (e.g. see Marra et al., 2022), we gauge-adjusted the radar data of each storm (defined as a consecutive wet period separated by 24 hours of dry weather across the whole study area) using data from the daily rain gauges described above (e.g. see Rinat et al., 2021). Despite these careful adjustments, the radar samples the study area about 3 km above the ground (see Marra et al. 2022) so that rainfall at the ground could be misplaced of a few hundreds of meters in case of strong winds in the lower atmosphere. This may cause some errors in the estimation of rain intensities; in particular, because of the typical characteristics of debris-flow convective rainfall (Marra et al., 2016), we expect that in these cases, our evaluation could be underestimated. While this does not affect our findings, some caution is to be used on the rain intensity values we report. It is worth noting that the previous studies in the region (e.g., Ben David-Novak et al., 2004) were based on data from a different weather radar, which was however located not far from the one used here; thus, the same caveats are to be used in interpreting those quantitative estimates.

4.2 Identification of the most likely triggering storms

Since the study area was documented (by airborne LiDAR) roughly every second year, we search for all the potential storms that could trigger the SLDFs during the time intervals between two subsequent scans (Fig. 3). For the analysis, we consider the location of each SLDF at the center of its mapped deposit. The many streams that drain the cliff have a very small drainage area (maximum distance between the deposits and the basin head 750 m). As the weather radar resolution is 500x500 m^2, we can assume that the rainfall observed by the radar in correspondence to the deposit location represents a good approximation of the rainfall over the drainage basin (Marra et al., 2014).

https://doi.org/10.5194/nhess-2022-184
Preprint. Discussion started: 20 July 2022


Natural Hazards and Earth System Sciences Discussions

195 Following this procedure, we plot for each SLDF, the five-minute rainfall intensity versus time, for its relevant two years interval (Fig. 3). For example, for a SLDF from group number three, mapped east to Metsoke Dragot, we used the radar data for the years 2013-2015. Note that gaps in the radar data are possible because of technical issues, and because during dry periods the radar is often turned off. In order to make sure that we did not miss a critical event, we compared the radar data with rain gauge stations. During the period of 2013-2017, we found only two storms (Jan 8-9, 2016 and Jan 27-29, 2017)
200 during which the radar was off.

We picked potential triggering events, by isolating those storms in which the peak rainfall intensities exceeded 10 mm h^{-1}, and the peak 30-minute intensity (average intensity over 30 minutes periods) exceeded 5 mm h^{-1} (Fig. 3). Recalling that previous studies reported thresholds of 30 mm h^{-1} over 1-hour periods and that 10 mm h^{-1} is often regarded as a threshold for defining convective precipitation (e.g., Peleg and Morin 2012), this selection is based on rather low intensities: it ensures we will select
205 all the potentially triggering storms and it diminishes the possible impact of radar underestimation mentioned above. It is worth noting that this selection is only based on intensity and no condition on the antecedent rainfall is used.

In total, we identify 14 potential storms that satisfy the above intensity conditions over the SLDFs during the periods of interest (Table 1). Nevertheless, only eight of these fourteen turned out to be potential events for all the mapped SLDFs of a group of interest (marked by red in Table 1 and blue rectangles in Fig. 3). Note, that one storm (Oct 26-29, 2015) is potential trigger for
210 the SLDFs of two groups.

https://doi.org/10.5194/nhess-2022-184
Preprint. Discussion started: 20 July 2022

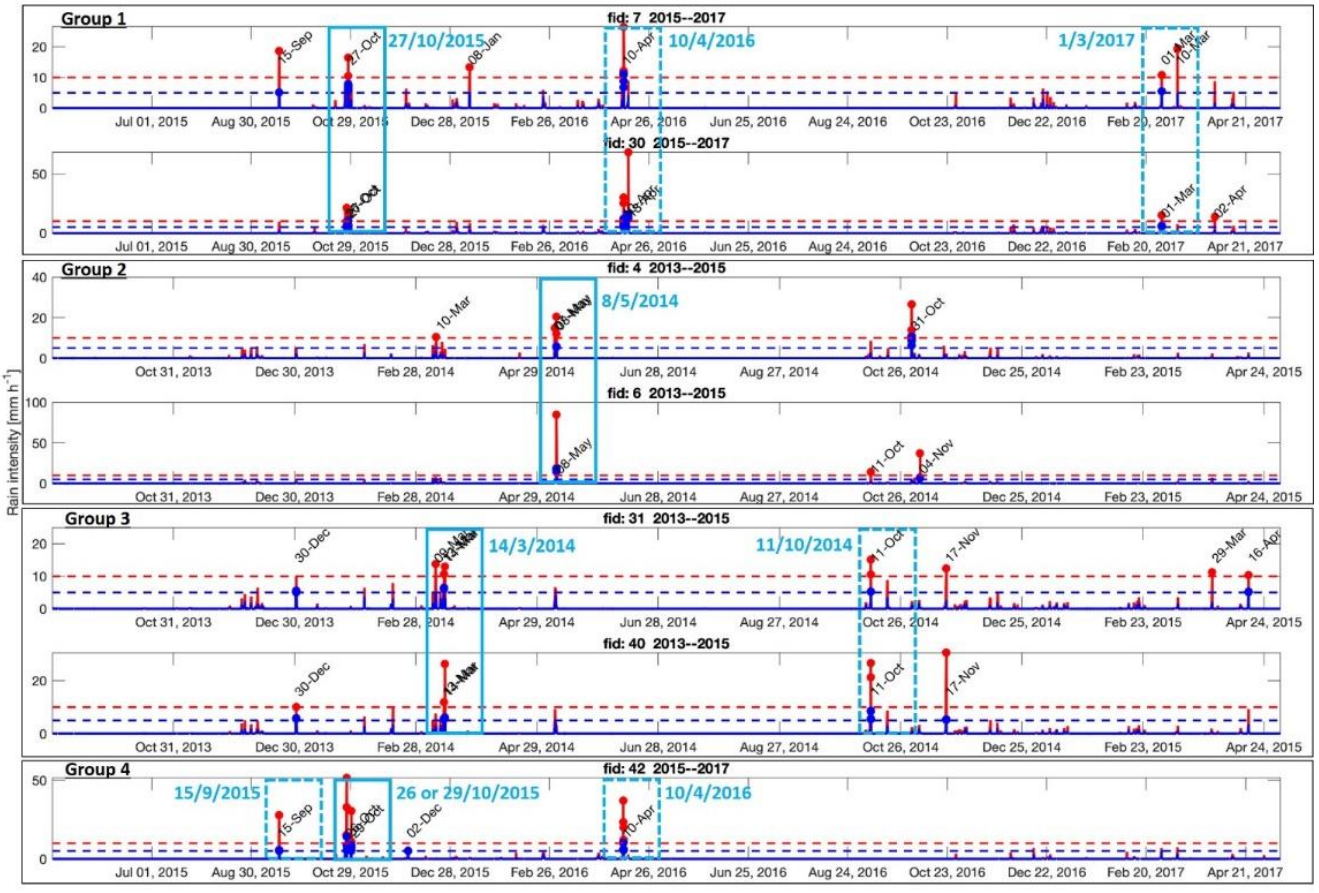

Figure 3: Time series of rainfall events over the four groups of SLDFs. Seven sub-plots of the rainfall intensity versus time (for two-year interval) for four different SLDF. In each sub-plot two graphs are shown: the rain intensity in 5 min interval (in red) and the smoothed intensity over a 30 min window (in blue). Horizontal lines mark two thresholds of 10 mm h-1 (red) and 5 mm h-1 (blue). Any storm during which the 5-min intensity overcomes the former thresholds or the 30-min overcomes the latter is marked by a circle. Rainfall events exceeding both thresholds for all the SLDFs of a group are marked by dashed light blue lines and are highlighted in Table 1. Continuous light blue lines indicate the suspected triggering storm.

https://doi.org/10.5194/nhess-2022-184
Preprint. Discussion started: 20 July 2022

Natural Hazards and Earth System Sciences Discussions

Table 1. Potential triggering storms and suspected triggering convective cells for the 43 SLDFs (numbered by Fid), organized into four groups. The weather system that produced the triggering cell is also reported.

Group number	Fid (mapped SLDFs)	Location	Potentially triggering storms	Suspected triggering cell	Weather system of the triggering cell
1	7-30	Qumran - Ein-Feshkha	15/9/2015 26-27/10/2015 10-13/4/2016 1/3/2017	27/10/2015, 13:55-14:40	Active Red Sea Trough[a]
2	0-6	Ovnat area	8/5/2014 31/10-4/11 /2014	8/5/2014, 13:50-14:10	Tropical Plume[b]
3	31-40	Metsoke Dragot	30/12/2013 13-14/3/2014 11/10/2014 17/11/2014 16/4/2015	14/3/2014, 10:35-10:55	Mediterranean Cyclone (with anomalous southern track)
4	41-42	Yishay valley	15/9/2015 26-29/10/2015 10/4/2016	26/10/2015, 15:35-15:55	Active Red Sea Trough[a]

[a] See also Marra and Morin (2018).
[b] See also Armon et al. (2018).

Once we identified the potential triggering rainstorms, we need to narrow down our choice to the most probable storm that triggered each SLDF group. To achieve that, we used additional analysis of the radar data, orthophotos, and online reports from social media and news websites. For each of the nine potential triggering rainstorms we examined the event time series in terms of total rainfall and rainfall intensity versus time, for a period of hours to a few days (Fig. 4), and we produced the 5-minute resolution rain intensity maps such as the one shown in Fig. 5. Using those, we followed the candidate convective cells in time and examined their spatiotemporal behavior with respect to (i) the mapped deposits and (ii) areas with similar slopes/sediment availability but no observed DF, narrowing our choice. In some cases, such as group 1 in the northern part of the study area, we could not clearly pinpoint a single cell that triggered the SLDFs in the group, and we needed to use additional information. Using two orthophotos from the years 2015-2016 we limit our search for two out of three rainstorm events: Oct 26-27, 2015 and Apr 10-13, 2016 (Table 1). Using a Facebook video showing deposits on the main road (route #90) (https://www.facebook.com/chen.sason.75/videos/1155321937831332, last accessed: Apr 25, 2022), where the road crosses

https://doi.org/10.5194/nhess-2022-184
Preprint. Discussion started: 20 July 2022

Natural Hazards and Earth System Sciences
Discussions

the most southern stream of mapped deposits from group 1, we could pinpoint a specific event and convective cell that most likely triggered group 1 SLDFs: Oct 27, 2015 between 13:55-14:40. In the video, one can see the sediments including boulders of tens of centimeters in diameter together with smaller fragments within mud, that suggest a hyper-concentrated or DF. Combining the above information, we ended up identifying four convective cells that, based on the information at our hand, most likely triggered the SLDFs in the four groups (Table 1, right column).

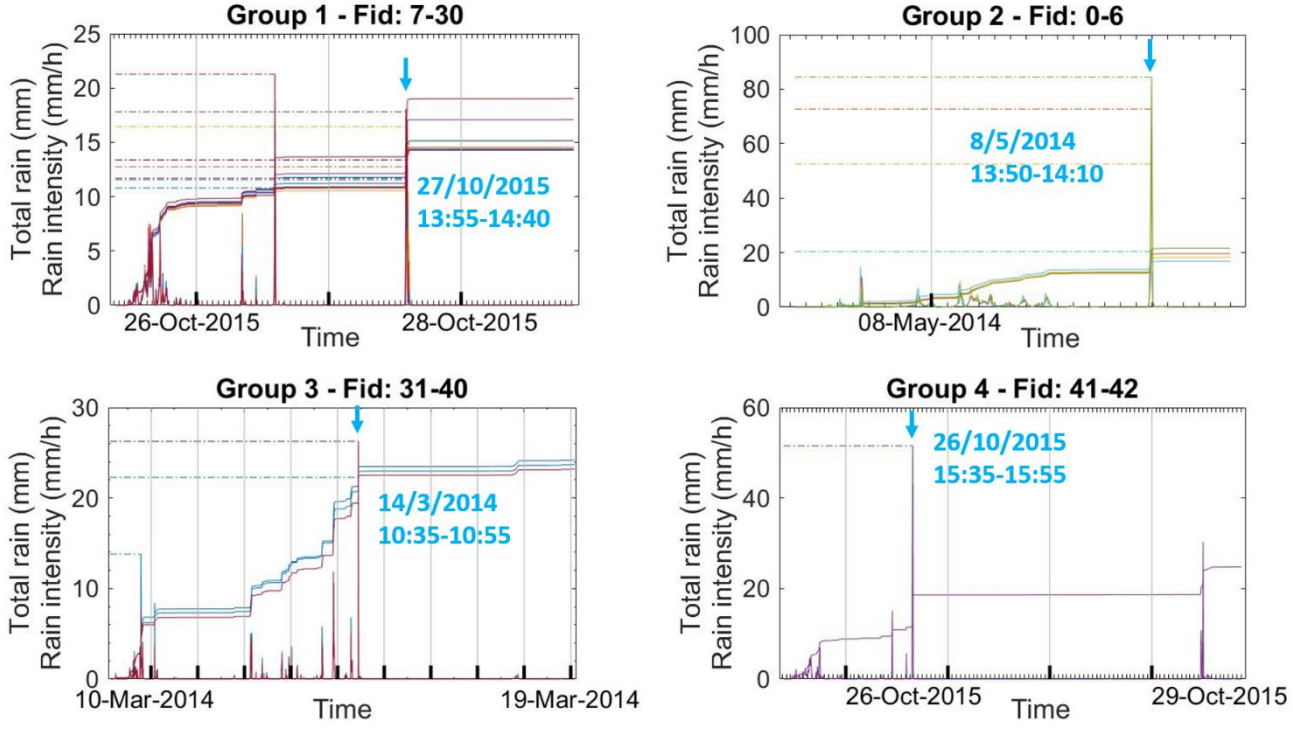

Figure 4: Rainfall evolution over the SLDF locations during the triggering storms (see Table 1). For each group we plot the intensity (spikes) and cumulative rain (stairs graph) during the storm, for all SLDF locations in the group (the different line colors). Dashed lines mark the peaks of rain intensity. A blue arrow marks the triggering cell during the storm. Note, that the y-axis shows both rain intensity in mm h^{-1} and total cumulative rain during the storm in mm.

https://doi.org/10.5194/nhess-2022-184
Preprint. Discussion started: 20 July 2022

Natural Hazards and Earth System Sciences
Discussions

4.3 Characterization of the triggering rainfall

The characteristics of the triggering rainfall were examined to evaluate the critical conditions for SLDF triggering in the study area. The triggering cells are intense and short, intensities are in the range of 10-85 mm h^{-1}, and durations between ~20 min (groups 2-4) and ~45 min (group 1, Table 1 and Fig. 4). Both, rainfall intensities and durations are lower than the previously suggested threshold for DF triggering in the study area (intensities >30 mm h^{-1} for duration of one hour or longer, (Ben David-Novak et al., 2004)), but underestimation in the weather radar data cannot be excluded. Interestingly, for all SLDFs significant rainfall was observed during the hours preceding the triggering cell (usually more than 10 mm, Fig. 4).

To further explore this point, we plot the spatial distribution of antecedent rain over the study area and compare it to the spatial distribution of the total rainfall yield of the cell, and of its maximum intensities over 5- and 30-min intervals (Fig. 6). Note, that the antecedent rain for these maps is defined as the time passed between the beginning of the storm and the time defined as the onset of the triggering convective cell. Figures 6b through 6d present the triggering cell characteristics (in the center of the map), and suggest that two additional convective cells (warmer colors) north and south to the main cell passed through the map area at the same time. While the maximum intensities of all three cells exceeds 10 mm h^{-1}, only the central one triggered the SLDFs (group 3). We suggest that although the southern cell well covers the steep slopes (meet the steep slope and sediment conditions) and is similar in rainfall intensities, no SLDF triggered, as the total amount of antecedent rain at this location was relatively small. Differently, for the northern cell it seems that the antecedent rain condition is met, but the cell overlap the steep slopes only on its edge (the cell at its peak intensity did not cross the cliff area).

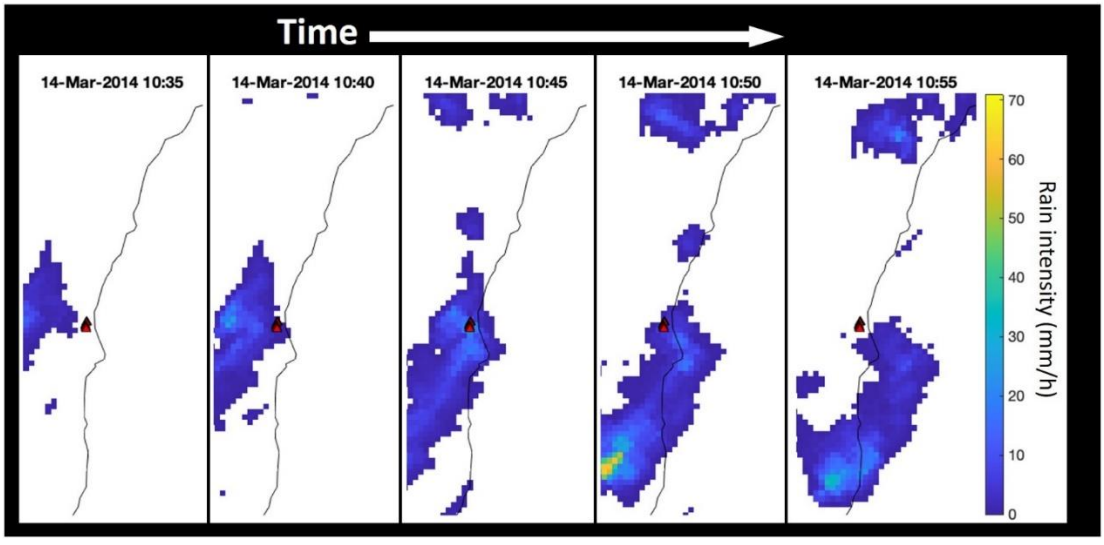

Figure 5: Weather radar maps. Time snapshots (time increases rightward) of the rain intensity over the study area during the time of the convective rain cell that triggered group 3 SLDFs (red rectangles). A black line marks the Dead-Sea shoreline. The highest rain intensities overlap the group SLDFs at 10:45 while the whole event is shorter than 30 min.

https://doi.org/10.5194/nhess-2022-184
Preprint. Discussion started: 20 July 2022

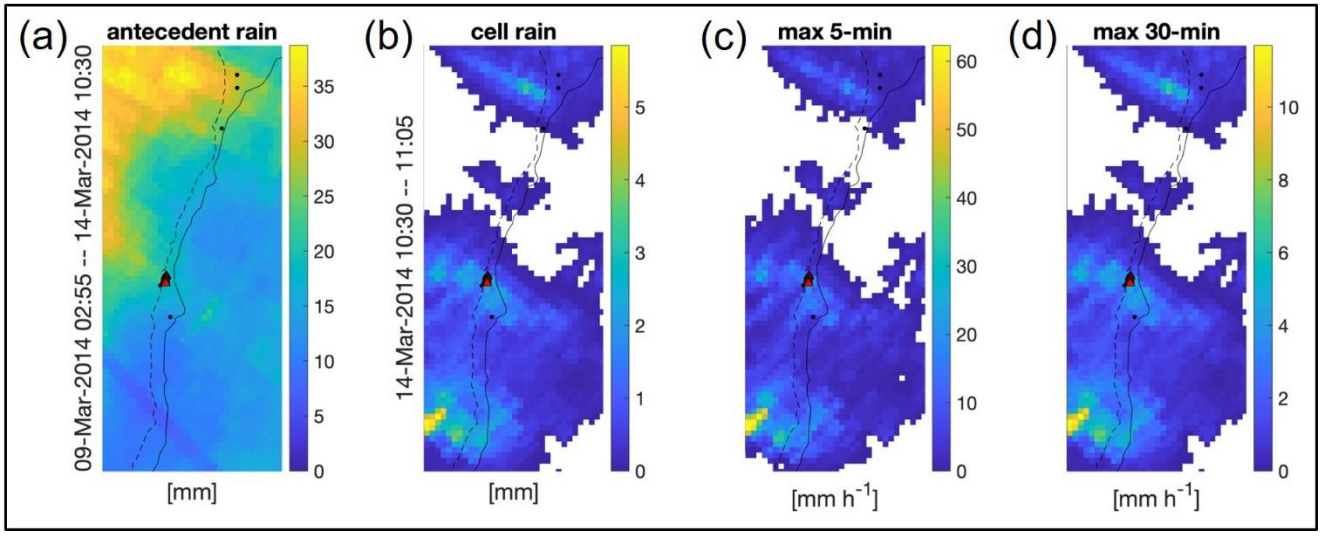

Figure 6: Rain map analyses of the triggering event shown in Fig. 5. The cliff-top (dashed line) together with the Dead Sea shoreline mark the narrow band of steep escarpment where debris flows may potentially triggered. (a) Antecedent rainfall – map of the total rainfall during the March 2014 event until the onset of the trigging convective cell rainfall. (b) The total rain fell during the triggering cell period (10:30-11:05). (c) Peak intensity maps of 5 min interval. (d) Peak intensity maps of the 5 min interval smoothed over 30 min window.

5 Discussion

5.1 The role of antecedent rainfall

The possible importance of antecedent rainfall on landslide triggering was extensively studied for non-arid environments (e.g. Glade et al. 2000; Aleotti 2004; Guzzetti et al. 2008; Frattini et al. 2009; Kim et al. 2021). In tropical areas (Brand, 1992) and slopes covered by grains having large inter-particle void space (Corominas and Moya, 1999), antecedent rainfall is less important than in other environments, possibly because of the high permeability of the local soils that reduces the potential for failure (Rahardjo et al., 2001). Conversely, to the best of our knowledge, the effect of antecedent rainfall on DF triggering in arid regions was not yet explored, probably due to the lack of DF observations and of adequate rainfall data.

We speculate that the antecedent rainfall or pre-flow of water in the steep channels caused by the antecedent rain could reduce the sediment strength by wetting. The reduction of sediment strength may be followed by enhanced incision or direct failure of the sediments within the channel. Such slope instability will initiate the SLDFs once the rainfall triggering convective cell will cause a significant water flow at these channels. Shmilovitz et al. (2020) showed that the threshold for runoff flow on nearby desert slopes is ~14-22 mm h^{-1} for a duration of five minutes. This threshold is met by the four convective cells that are considered to trigger all the mapped SLDF deposits in this study but it is also met by other storms among the ones we identify as possible candidates (Table 1). We hypothesize, that due to the lack of antecedent rainfall preceding the main

https://doi.org/10.5194/nhess-2022-184
Preprint. Discussion started: 20 July 2022

Natural Hazards and Earth System Sciences
Discussions

convective cells, no SLDFs were triggered by the latter storms. At the same time, flash floods could indeed have been generated, as frequently observed along the cliff during heavy storms (Belachsen et al., 2017).

In order to validate the hypothesis that antecedent rainfall is an important factor in SLDF triggering in the study area, we examined the whole period between 2013 and 2019 with the aim of identifying storms which could potentially trigger SLDFs in terms of rain intensity, but did not. We focused on the triggering locations of our SLDFs, in order to ensure the susceptibility conditions are met. In Fig. 7 we plot the antecedent rainfall versus the 5-minute rain intensity for a representative SLDF deposit from each group. Here, the antecedent rainfall is calculated as all the rain accumulated on the deposit pixel during the period starting on a 24 h break in rain and until the specific measured intensity. For most cases, in these new graphs we picked the same potential triggering events as we previously showed (Table 1). Interestingly, for extreme intensity rainfall events (>60 mm h^{-1}), like Sep 15, 2015 event in group 2 (Fig. 7b) and events on Jun 4, 2018 and Oct 29, 2015 in group 3 (Fig. 7c), no SLDF deposits were observed, even after re-checking the target area in our DSM differences.

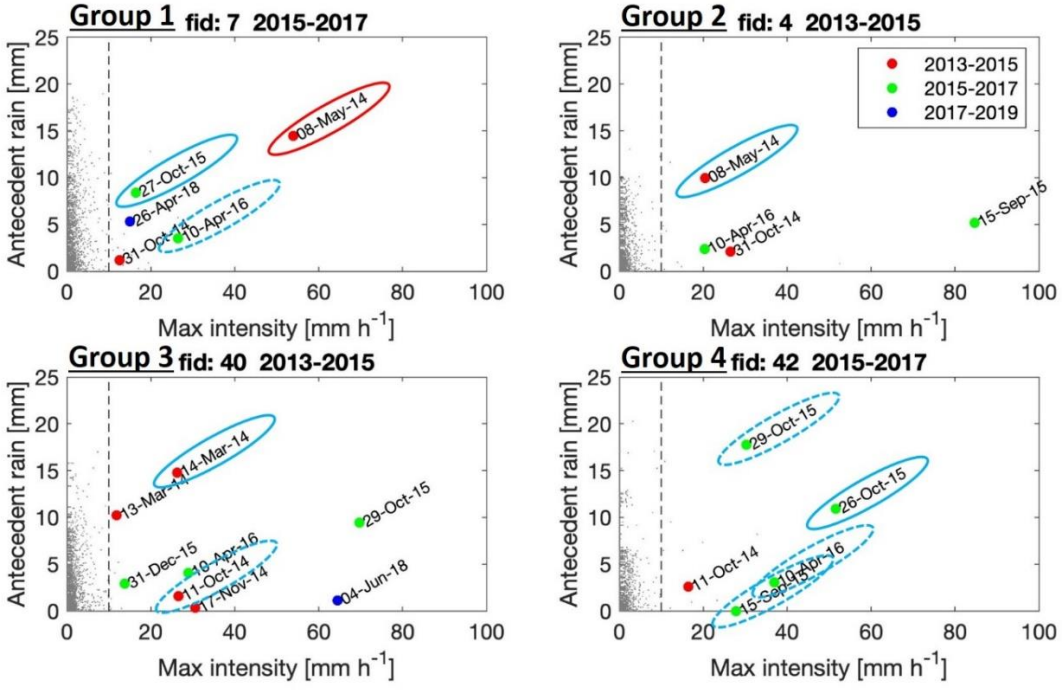

Figure 7: Scatter plots of antecedent rainfall versus maximum 5-minute rain intensity observed over four SLDFs representative of the four groups for all the storms observed in the radar archive in the period 2013-2019. Data points exceeding the intensity of 10 mm h^{-1} for 5-minute intensity and 5 mm h^{-1} for 30-minute intensity are marked by color and classified according to the time interval specified by the elevation-difference maps. Potentially triggering storms (red text in Table 1) are marked with dashed blue ellipses, whereas the most likely triggering storm identified in this study is marked with a continuous blue ellipse. The red ellipse in group 1 marks the storm of May 8 2014, discussed in Section 5.1.

https://doi.org/10.5194/nhess-2022-184
Preprint. Discussion started: 20 July 2022


Natural Hazards and Earth System Sciences Discussions

An interesting additional story is told by Fig. 7a: the event on May 8, 2014 shows relatively high antecedent rainfall (>10 mm) as well as peak intensity (>50 mm h^{-1}), compared to the likely triggering event on Oct 27, 2015, but occurred before the SLDFs in group 1 were triggered (they were not observed in the LiDAR flight between these two storms). Given the strong characteristics of this cell in terms of both antecedent rainfall and peak intensity, and since the mapping could not be fully effective for small DFs, we further examined the region around group 1 looking for potential signatures of the May 8, 2014 storm. Indeed, some tiny shallow deposits appeared during the period 2013-2015. They are located on the western edge of group 1 area, in close proximity to the May 8, 2014 cell peak. While these mass movements are small with respect to the SLDFs examined so far in this paper, they show similar DF-like properties. The fact that we could find new mass movements based on the requirement of both antecedent rainfall and peak intensity constitutes an additional element supporting our hypothesis.

5.2 Implications for debris flow frequency and a future early warning systems in the region

The need for antecedent rainfall could also help explaining the low incidence of DFs in the area: to date, only seven modern debris-flow triggering storms are reported in the study area. Four events reported for ten years period between October 1987 to October 1997 (Ben David-Novak, 1998; Ben David-Novak et al., 2004) and three identified in the current study – roughly equivalent to one triggering storm every two-three years. So far, the rarity of DFs in the area was explained by the dry weather (i.e., low number of storms) and the small areal extent of the susceptible steep slopes: only convective cells hitting the small susceptible area can trigger a DF. However, while storms in the area are indeed not frequent, each storm usually brings numerous convective cells. Belachsen et al. (2017) identified 424 storms in the area in the period 1990-2014, about ~20 per year, associated with over 10,000 convective cells, an average of >24 cells per storm. Similarly, Marra and Morin (2018) showed that individual storms can bring even hundreds of high-intensity convective cells. With these numbers, it is more difficult to motivate the rarity of DFs just using the reasoning above. Conversely, the here suggested need for antecedent rainfall as a prerequisite for the triggering implies a need for an intense convective cell to hit an area where non-negligible rainfall already occurred during the same storm, or within the short time needed for the slopes to dry in the desert climate of the dry days.

The need for antecedent rainfall as a critical triggering condition also in arid areas could help simplifying the prediction of such events. Heavy rain intensity remains a key trigger of DFs, but the trajectory and intensity of convective cells cannot be forecasted with sufficient accuracy even with the most advanced weather models (e.g., see Rinat et al., 2021). In addition, the short distance between the debris sources and the vulnerable structures drastically reduces the effectiveness of warnings based on radar nowcasting (e.g., Sideris et al., 2020). Conversely, antecedent rainfall can be monitored during the storm using weather radar observations, and used to highlight areas more susceptible to possible incoming convective cells. This information could be used to send targeted warnings to the relevant locations and structures at risk.

https://doi.org/10.5194/nhess-2022-184
Preprint. Discussion started: 20 July 2022


Natural Hazards and Earth System Sciences
Discussions

6 Conclusions

In this paper, we investigate the rainfall conditions leading to DFs in steep arid slopes, where the lack of DF observations and rainfall data still hinders our understanding of the typical triggering conditions. We use high-resolution topography, field surveys and social media information to map over 40 deposits resulted from short-lived debris flows (SLDFs) in the arid region of the Dead Sea western escarpment during 2013-2019. We then use high-resolution weather radar rainfall estimates to investigate the triggering rainfall conditions in terms of peak intensity and rainfall amounts prior to the triggering convective cell.

The spatial and temporal analysis of the mapped deposits and of weather radar data over the triggering locations, suggests that the 43 identified SLDFs were triggered by three storms occurred during the spring of 2014 and the autumn of 2015. The mapped deposits were likely triggered by short convective cells which usually lasted less than 30 minutes and could show peak intensities lower than 30 mm h^{-1}. These numbers are lower compared to previous studies based on two events in the area (>30 mm h^{-1} for >1 hour). Comparing triggering and non-triggering storms, we suggest that antecedent rainfall during the hours to days prior to the triggering convective cells may play a critical role for DF triggering in arid steep slopes. We speculate that wetting of the slope sediments reduces it strength and allows its massive drift during the channel flow caused by the main convective cell. Our hypothesis is supported by the observation of numerous convective cells with intensities similar or greater than the triggering ones but no SLDF signature in the topography even in susceptible locations such as the location of SLDFs triggered by subsequent storms. In addition, our hypothesis could help explaining the very low occurrence frequency of DFs in an area with high susceptibility and relatively frequent high-intensity convective cells. Our findings bring new information to our understanding of DF triggering in arid regions and could be included in regional-scale warning systems to help minimizing the hazard potential of these events.

https://doi.org/10.5194/nhess-2022-184
Preprint. Discussion started: 20 July 2022


Natural Hazards and Earth System Sciences Discussions

Data availability

Raingauge data were provided and pre-processed by the Israel Meteorological Service and are freely available at https://ims.data.gov.il/ (last access: 13 March 2022, Hebrew only). Corrected weather radar data were made available by the Hydrometeorology lab at the Hebrew University of Jerusalem and cannot be directly shared by the authors; the data can be requested to the Hydrometeorology lab at https://hydrometeorology-lab.huji.ac.il/book/contact-us (last accessed 28 June 2022). Orthophotos are the product of the Survey of Israel, and are available according to their policy. For further information, please contact the Survey by email: tatsa@mapi.gov.il. Airborne LiDAR scans ordered by the Geological Survey of Israel from Ofek Aerial Photography. The original scans cannot be shared online. Please contact the corresponding author for further information.

Author contribution

SST conducted mapping and fieldwork, data curation and formal analysis, funding acquisition, and wrote the original draft. FM was responsible for rainfall data curation and formal analysis. Both authors conceptualized the study and contributed to the writing – review & editing.

Competing interests

The authors declare that they have no conflict of interest.

Acknowledgments

We thank Efrat Morin, Yehuda Enzel and Oded Katz for fruitful discussions and Moshe Armon for the synoptic classification of the storms. We also thank Yair Rinat, Hallel Lutsky, and Jonathan Levy for their assistance in the field work. This work was funded by the Geological Survey of Israel, Dead-Sea project #40832. FM was supported by internal funds of the Institute of Atmospheric Sciences and Climate of the National Research Council of Italy (CNR-ISAC).

https://doi.org/10.5194/nhess-2022-184
Preprint. Discussion started: 20 July 2022

References

Ahlborn, M., Armon, M., Ben Dor, Y., Neugebauer, I., Schwab, M. J., Tjallingii, R., Shoqeir, J. H., Morin, E., Enzel, Y., and Brauer, A.: Increased frequency of torrential rainstorms during a regional late Holocene eastern Mediterranean drought, Quaternary Research (United States), 89, 425–431, https://doi.org/10.1017/qua.2018.9, 2018.

Aleotti, P.: A warning system for rainfall-induced shallow failures, Engineering Geology, 73, 247–265, https://doi.org/10.1016/j.enggeo.2004.01.007, 2004.

Armon, M., Dente, E., Smith, J. A., Enzel, Y., and Morin, E.: Synoptic-scale control over modern rainfall and flood patterns in the Levant drylands with implications for past climates, Journal of Hydrometeorology, 19, 1077–1096, https://doi.org/10.1175/JHM-D-18-0013.1, 2018.

Armon, M., Morin, E., and Enzel, Y.: Overview of modern atmospheric patterns controlling rainfall and floods into the Dead Sea: Implications for the lake's sedimentology and paleohydrology, Quaternary Science Reviews, 216, 58–73, https://doi.org/https://doi.org/10.1016/j.quascirev.2019.06.005, 2019.

Bartov, Y., Stein, M., Enzel, Y., Agnon, A., and Reches, Z.: Lake levels and sequence stratigraphy of Lake Lisan, the late Pleistocene precursor of the Dead Sea, Quaternary Research, 57, 9–21, https://doi.org/10.1006/qres.2001.2284, 2002.

Bartov, Y., Enzel, Y., Porat, N., and Stein, M.: Evolution of the Late Pleistocene-Holocene Dead Sea basin from sequence statigraphy of fan deltas and lake-level reconstruction, Journal of Sedimentary Research, 77, 680–692, https://doi.org/10.2110/jsr.2007.070, 2007.

Begin, Z. B., Nathan, Y., and Ehrlich, A.: Stratigraphy and facies distribution in the Lisan Formation—new evidence from the area south of the Dead Sea, Israel, Israel Journal of Earth Sciences, 29, 182–189, 1980.

Belachsen, I., Marra, F., Peleg, N., and Morin, E.: Convective rainfall in a dry climate: Relations with synoptic systems and flash-flood generation in the Dead Sea region, Hydrology and Earth System Sciences, 21, 5165–5180, https://doi.org/10.5194/hess-21-5165-2017, 2017.

Blackwelder, E.: Mudflow as a geologic agent in semiarid mountains, Bulletin of the Geological Society of America, 39, 465–484, https://doi.org/10.1130/GSAB-39-465, 1928.

Brand, E. W.: Slope instability in tropical areas., in: Proceedings of the 6th International Symposium on Landslides, 2031–2051, 1992.

Caine, N.: The rainfall intensity-duration control of shallow landslides and debris flows., Geografiska Annaler Series A, 62, 23–27, https://doi.org/10.1080/04353676.1980.11879996, 1980.

Church, M. and Miles, M. J.: Meteorological antecedents to debris flow in southwestern British Columbia; some case studies, Reviews in Engineering Geology, IVV, 63–80, 1987.

Coe, J. A., Glancy, P. A., and Whitney, J. W.: Volumetric analysis and hydrologic characterization of a modern debris flow near Yucca Mountain, Nevada, Geomorphology, 20, 11–28, https://doi.org/10.1016/s0169-555x(97)00008-1, 1997.

Corominas, J. and Moya, J.: Reconstructing recent landslide activity in relation to rainfall in the Llobregat River basin, Eastern Pyrenees, Spain, Geomorphology, 30, 79–93, https://doi.org/10.1016/S0169-555X(99)00046-X, 1999.

Costa, J. E.: Rheologic, geomorphic, and sedimentologic differentiation of water floods, hyperconcentrated flows, and debris

flows, Flood geomorphology, 113–122, 1988.

Ben David-Novak, H.: Modern and Holocene debris flows along the western escarpment of the Dead-Sea (in Hebrew), The Hebrew University of Jerusalem, 129 pp., 1998.

Ben David-Novak, H., Morin, E., and Enzel, Y.: Modern extreme storms and the rainfall thresholds for initiating debris flow on the hyperarid western escarpment of the Dead Sea, Israel, Bulletin of the Geological Society of America, 116, 718–728, https://doi.org/10.1130/B25403.2, 2004.

Destro, E., Marra, F., Nikolopoulos, E. I., Zoccatelli, D., Creutin, J. D., and Borga, M.: Spatial estimation of debris flows-triggering rainfall and its dependence on rainfall return period, Geomorphology, 278, 269–279, https://doi.org/10.1016/j.geomorph.2016.11.019, 2017.

Dunkerley, D.: Rainfall intensity in geomorphology: Challenges and opportunities, Progress in Physical Geography, 45, 488–513, https://doi.org/10.1177/0309133320967893, 2021.

Enzel, Y.: Holocene debris flows along the western escarpment of the Dead Sea basin: Israel Ministry of Infrastructure, Earth Sciences Administration Report ES-53-2001 (in Hebrew), 28 pp., 2001.

Frattini, P., Crosta, G., and Sosio, R.: Approaches for defining thresholds and return periods for rainfall-triggered shallow landslides, Hydrological Processes, 23, 1444–1460, https://doi.org/10.1002/hyp.7269, 2009.

Garfunkel, Z. and Ben-Avraham, Z.: The structure of the Dead Sea basin, Tectonophysics, 266, 155–176, 1996.

Garfunkel, Z., Zak, I., and Freund, R.: Active faulting in the dead sea rift, Tectonophysics, 80, 1–26, 1981.

Glade, T., Crozier, M., and Smith, P.: Applying probability determination to refine landslide-triggering rainfall thresholds using an empirical "Antecedent Daily Rainfall Model," Pure and Applied Geophysics, 157, 1059–1079, https://doi.org/10.1007/s000240050017, 2000.

Griffiths, P. G.: Frequency and initiation of debris flows in Grand Canyon, Arizona, Journal of Geophysical Research, 109, https://doi.org/10.1029/2003jf000077, 2004.

Guzzetti, F., Peruccacci, S., Rossi, M., and Stark, C. P.: The rainfall intensity-duration control of shallow landslides and debris flows: An update, Landslides, 5, 3–17, https://doi.org/10.1007/s10346-007-0112-1, 2008.

Haviv, I., Enzel, Y., Whipple, K. X., Zilberman, E., Stone, J., Matmon, A., and Fifield, L. K.: Amplified erosion above waterfalls and oversteepened bedrock reaches, Journal of Geophysical Research: Earth Surface, 111, https://doi.org/10.1029/2006JF000461, 2006.

Hochman, A., Marra, F., Messori, G., Pinto, J. G., Raveh-Rubin, S., Yosef, Y., and Zittis, G.: Extreme weather and societal impacts in the eastern Mediterranean, Earth System Dynamics, 13, 749–777, https://doi.org/10.5194/esd-13-749-2022, 2022.

Iverson, R. M.: The physics of debris flows, Reviews of Geophysics, 35, 245–296, https://doi.org/10.1029/97RG00426, 1997.

Iverson, R. M.: Landslide triggering by rain infiltration, Water Resources Research, 36, 1897–1910, https://doi.org/10.1029/2000WR900090, 2000.

Kim, S. W., Chun, K. W., Kim, M., Catani, F., Choi, B., and Seo, J. Il: Effect of antecedent rainfall conditions and their variations on shallow landslide-triggering rainfall thresholds in South Korea, Landslides, 18, 569–582,

445 https://doi.org/10.1007/s10346-020-01505-4, 2021.

Marra, F. and Morin, E.: Use of radar QPE for the derivation of Intensity-Duration-Frequency curves in a range of climatic regimes, Journal of Hydrology, 531, 427–440, https://doi.org/10.1016/j.jhydrol.2015.08.064, 2015.

Marra, F. and Morin, E.: Autocorrelation structure of convective rainfall in semiarid-arid climate derived from high-resolution X-Band radar estimates, Atmospheric Research, 200, 126–138, https://doi.org/10.1016/j.atmosres.2017.09.020, 2018.

450 Marra, F., Nikolopoulos, E. I., Creutin, J. D., and Borga, M.: Radar rainfall estimation for the identification of debris-flow occurrence thresholds, Journal of Hydrology, 519, 1607–1619, https://doi.org/10.1016/j.jhydrol.2014.09.039, 2014.

Marra, F., Nikolopoulos, E. I., Creutin, J. D., and Borga, M.: Space–time organization of debris flows-triggering rainfall and its effect on the identification of the rainfall threshold relationship, Journal of Hydrology, 541, 246–255, https://doi.org/10.1016/j.jhydrol.2015.10.010, 2016.

455 Marra, F., Armon, M., and Morin, E.: Coastal and orographic effects on extreme precipitation revealed by weather radar observations, Hydrology and Earth System Sciences, 26, 1439–1458, https://doi.org/10.5194/hess-26-1439-2022, 2022.

Melis, T. S. and Webb, R. H.: Debris flows in Grand Canyon National Park, Arizona: magnitude, frequency and effects on the Colorado River, in: Proceedings - National Conference on Hydraulic Engineering, 1290–1295, 1993.

Melis, T. S., Webb, R. H., Griffiths, P. G., and Wise, T. W.: Magnitude and frequency data for historic debris flows in Grand
460 Canyon National Park and vicinity, Arizona, U. S. Geological Water-Resources Investigations Report 94-4214, 285 pp., 1994.

Mor, U.: The geology of the Judean Desert in the area of Nahal Darga (in Hebrew), GSI/21/87, Jerusalem, 112 pp., 1987.

Mostbauer, K., Kaitna, R., Prenner, D., and Hrachowitz, M.: The temporally varying roles of rainfall, snowmelt and soil moisture for debris flow initiation in a snow-dominated system, Hydrology and Earth System Sciences, 22, 3493–3513, https://doi.org/10.5194/hess-22-3493-2018, 2018.

465 Peleg, N. and Morin, E.: Convective rain cells: Radar-derived spatiotemporal characteristics and synoptic patterns over the eastern Mediterranean, Journal of Geophysical Research (Atmospheres), 117, D15116, https://doi.org/10.1029/2011JD017353, 2012.

Pierson, T.: Distinguishing between debris flows and floods from field evidence in small watersheds, Water, 4, 2005.

Rahardjo, H., Li, X. W., Toll, D. G., and Leong, E. C.: The effect of antecedent rainfall on slope stability, Geotechnical and
470 Geological Engineering, 19, 371–399, https://doi.org/10.1023/A:1013129725263, 2001.

Raz, E.: The geology of the Judean Desert, Ein Gedi area (in Hebrew), GSI\S3\1983, Jerusalem, 110 pp., 1983.

Rinat, Y., Marra, F., Armon, M., Metzger, A., Levi, Y., Khain, P., Vadislavsky, E., Rosensaft, M., and Morin, E.: Hydrometeorological analysis and forecasting of a 3-day flash-flood-triggering desert rainstorm, Natural Hazards and Earth System Sciences, 21, 917–939, https://doi.org/10.5194/nhess-21-917-2021, 2021.

475 Roth, I.: The geology Wadi el-Qilt area (in Hebrew), M.Sc. thesis, The Hebrew University of Jerusalem, 82 pp., 1969.

Shmilovitz, Y., Morin, E., Rinat, Y., Haviv, I., Carmi, G., Mushkin, A., and Enzel, Y.: Linking frequency of rainstorms, runoff generation and sediment transport across hyperarid talus-pediment slopes, Earth Surface Processes and Landforms, 45, 1644–1659, https://doi.org/10.1002/esp.4836, 2020.

https://doi.org/10.5194/nhess-2022-184
Preprint. Discussion started: 20 July 2022

Sideris, I. V, Foresti, L., Nerini, D., and Germann, U.: NowPrecip: localized precipitation nowcasting in the complex terrain of Switzerland, Quarterly Journal of the Royal Meteorological Society, 146, 1768–1800, https://doi.org/https://doi.org/10.1002/qj.3766, 2020.

Sneh, A.: Late Pleistocene fan-deltas along the Dead Sea Rift, Society of Economic Paleontologists and Mineralogists Special Publication, 49, 541–552, 1979.

Sneh, A., Bartov, Y., and Weissbrod, T.: Stratigraphic chart of exposed rock-units in Israel, 2000.

Stolle, A., Langer, M., Blöthe, J. H., and Korup, O.: On predicting debris flows in arid mountain belts, Global and Planetary Change, 126, 1–13, https://doi.org/10.1016/j.gloplacha.2014.12.005, 2015.

Takahashi, T.: Debris Flow: Mechanics, Prediction and Countermeasures, 2nd edition, CRC Press, 572 pp., 2014.

Tubi, A. and Dayan, U.: Tropical Plumes over the Middle East: Climatology and synoptic conditions, Atmospheric Research, 145–146, 168–181, https://doi.org/10.1016/j.atmosres.2014.03.028, 2014.

Webb, R. H., Pringle, P. T., and Rink, G. R.: Debris Flows from Tributaries of the Colorado River, Grand Canyon National Park, Arizona, 1989.

Wells, S. G. and Harvey, A. M.: Sedimentologic and geomorphic variations in storm-generated alluvial fans, Howgill Fells, northwest England., Geological Society of America Bulletin, 98, 182–198, https://doi.org/10.1130/0016-7606(1987)98<182:SAGVIS>2.0.CO;2, 1987.

Zoccatelli, D., Marra, F., Armon, M., Rinat, Y., Smith, J. A., and Morin, E.: Contrasting rainfall-runoff characteristics of floods in desert and Mediterranean basins, Hydrology and Earth System Sciences, 23, 2665–2678, https://doi.org/10.5194/hess-23-2665-2019, 2019.